

**Building integration of photovoltaic power systems using
amorphous silicon modules: irradiation loss due to non-
conventional orientations**

N.J.C.M. van der Borg
E.J. Wiggelinkhuizen

Acknowledgement/Preface

Principal: Novem BV
Project number: 146.210-009.1
ECN project number: 7.4426

Abstract

In October 1998 an existing office building of ECN was retrofitted with four photovoltaic power systems with single junction amorphous silicon modules. The purposes of the retrofit and the corresponding monitoring activities were the following:

- demonstration of the applied technology for building integration,
- generation of general knowledge on irradiation in the built environment with non-optimal orientations,
- collection of specific knowledge on the applied PV-systems.

The monitoring data were used to validate generally available simulation models on the effects of orientation, shading, reflection, frequency distribution and spectral distribution of the irradiance. The results of the monitoring and of the modelling were combined to quantify the performance of the PV-systems.

The most important results are:

- Models are available for the quantification of the effect of orientation, shading, reflection and low irradiance. The models for shading were not validated sufficiently.
- The relevance of the spectral effect for a-Si has been demonstrated. A model for the quantification of its annual effect is not available.
- The performance was quantified of the PV-systems on the North, East, South and West façade.
- The modules show a beginning delamination after an operation period of 24 months.
- The inverters have performed properly. However a more appropriate selection of the inverter, based on the actual array power distribution rather than on the nominal array power, would increase the performance.

Key words

photovoltaic power systems, monitoring, modelling, amorphous silicon, façades, building integration

CONTENTS

1.	INTRODUCTION	5
2.	PV SYSTEMS	6
3.	MEASUREMENT EQUIPMENT	8
3.1	Monitoring system	8
3.2	IV-tracer and spectrometer	9
4.	SIMULATION TOOLS	10
5.	IRRADIATION	11
5.1	Data set	11
5.2	Reflection	11
5.2.1	Introduction	11
5.2.2	Model validation	12
5.2.3	Quantification of the reflection loss	13
5.3	Spectral effect	13
5.3.1	Introduction	13
5.3.2	Spectral response	14
5.3.3	Spectrum model	14
5.3.4	Quantification of the spectral effect	15
5.4	Diffuse irradiation on the horizontal plane	17
5.4.1	Introduction	17
5.4.2	Model validation	17
5.5	Irradiation on the tilted plane	18
5.5.1	Introduction	18
5.5.2	Model validation	18
5.5.3	Orientation loss	19
5.6	Shading	20
5.6.1	Introduction	20
5.6.2	Near shading (PVsyst)	20
5.6.3	Far shading (PVsyst)	21
5.6.4	Near shading (PVcad)	21
5.6.5	Discussion of the results	21
5.7	Observations concerning PVsyst	23
5.7.1	Perez model	23
5.7.2	Ground reflection	23
6.	TEMPERATURES	24
7.	ENERGY PRODUCTION	25
7.1	Measurements	25
7.2	Performance modelling	27
8.	SYSTEM RELIABILITY	30
9.	CONCLUSIONS	31
10.	REFERENCES	33
	APPENDICES	34

1. INTRODUCTION

In October 1998 an existing office building of ECN was retrofitted with four photovoltaic power systems. The PV-systems were mounted vertically against the North, East, South and West façades. In comparison with more conventional orientations little information is available on the possible irradiation effects for these non-optimal orientations in the built environment. Since it is expected that the number of building integrated PV-systems will increase in the future the PV-systems on the office building were used to study the effects of reflection, spectral response, shading, azimuth angle and tilt angle on the available irradiation.

With the financial support of NOVEM a monitoring programme was started in June 1999 (Novem project number 146.210-009.1) with a total duration of 2 years.

The purposes of the retrofit and the corresponding monitoring activities were the following.

- demonstration of the applied technology for building integration,
- generation of general knowledge on irradiation in the built environment with non-optimal orientations,
- collection of specific knowledge on the applied PV-systems.

The general knowledge on irradiation in the built environment was obtained by the validation of generally available simulation tools using measurement data obtained at the specific location. The PV-systems, the measurement equipment and the simulation tools are described in the chapters 2, 3 and 4 respectively. The results of the validation of models and simulation tools are given in chapter 5.

The specific knowledge on the temperatures, performance and reliability of the applied PV-systems is given in the chapters 6, 7 and 8 respectively.

In chapter 9 the conclusions are summarised.

2. PV SYSTEMS

Each of the four façades of the Renewable Energy Building of ECN is equipped with a PV-system. The four PV-systems are described in table 1.

façade =>	North	East	South	West
Azimuth angle	353°	83°	173°	263°
Tilt angle	90° (vertical)			
Module type	single junction a-Si 12 Wp; Fortum; 0.264 m ² cell area; frameless			
String	7 modules in series, $V_{mpp} \approx 112$ V (STC)			
Array	6 strings in parallel, $I_{mpp} \approx 4.5$ A; $P_{mpp} = 504$ W (STC)			
Inverter	SMA Sunny Boy SWR 700; 420 W _{ac} ; 75 - 150 V _{dc}			

Table 1: Description of the PV-systems.

The building with the PV-systems is shown in figure 1. Neighbouring buildings form obstacles in front of the North, East and South façade while the West façade has a free view towards the horizon (see figures 2a and 2b).

The geographical position of the building is 52° 45' Northern latitude; 4° 39' Eastern longitude.

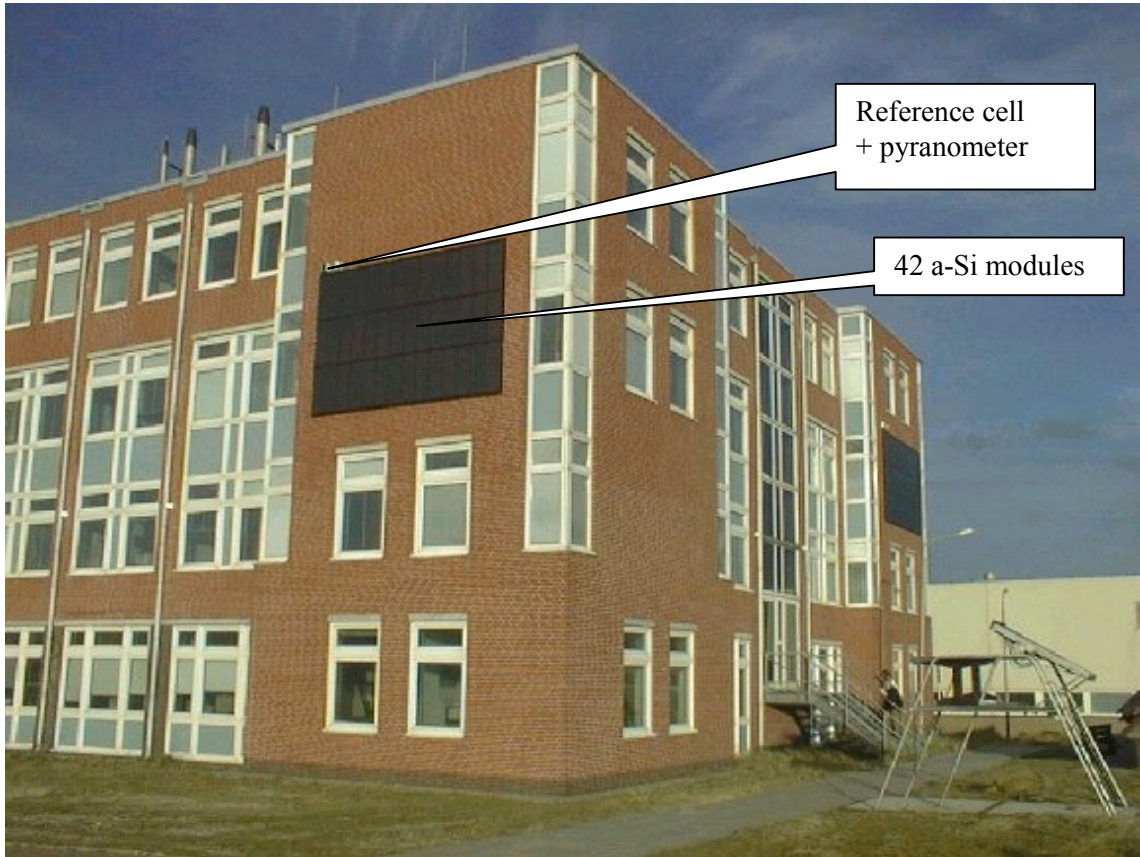


Figure 1: The Renewable Energy Building showing two of the four PV-systems



Figure 2a and 2b: View from the roof towards South-East (left) and West (right)

3. MEASUREMENT EQUIPMENT

3.1 Monitoring system

The monitoring system is based upon a measurement-PC that collects the measurement data with a sample frequency of 0.1 Hz during consecutive measurement periods of 10 minutes. The data of each measurement period are condensed into averaged values and stored for subsequent evaluation. The measurement data are provided by 5 decentralised data acquisition units, connected to the PC by a local operating network (LON), and by the monitoring facilities of the inverters, connected to the PC by an RS485/232 network. An overview of the measured quantities is given in table 2.

Quantity	sensor type	location	additional info
AC power North	inverter facility	North façade	inaccurate data
AC power East	inverter facility	East façade	inaccurate data
AC power South	inverter facility	South façade	inaccurate data
AC power West	inverter facility	West façade	inaccurate data
Global irradi. horiz.	pyranometer	Roof	
Diffuse irradi. horiz.	pyranometer	Roof	with shadow ring
Ambient temperature	AD590	Roof	
Irradiance North;pyr	pyranometer	North façade	
Irradiance North;cell	reference cell	North façade	Mc-Si & 4 mm KG5 filter
Module temp; North	AD590	North façade	Sensor on module rearside
Irradiance East;pyr	pyranometer	East façade	
Irradiance East;cell	reference cell	East façade	Mc-Si & 4 mm KG5 filter
Module temp; East	AD590	East façade	Sensor on module rearside
Irradiance South	pyranometer	South façade	
Irradiance South;cell	reference cell	South façade	Mc-Si & 4 mm KG5 filter
Module temp; South	AD590	South façade	Sensor on module rearside
Wall temp_1; South	AD590	South façade	sensor behind array
Wall temp_2; South	AD590	South façade	sensor beside array
Irradiance West	pyranometer	West façade	
Irradiance West;cell	reference cell	West façade	Mc-Si & 4 mm KG5 filter
Module temp; West	AD590	West façade	Sensor on module rearside
Wall temp_1; West	AD590	West façade	sensor behind array
Wall temp_2; West	AD590	West façade	sensor beside array

Table 2: Overview of the measured quantities

The pyranometers are of the type CM21 (Kipp & Zonen). The influence of the shadow ring on the measured diffuse irradiance was accounted for with the correction factors as provided by the manufacturer. Kipp & Zonen performed the calibrations.

The reference cells were made of mc-Si and are covered with a 4 mm thick KG5-filter (manufactured by Schott Glass Technologies) that acts as an infrared blocking filter (see paragraph 5.3.2). The calibrations were performed by ECN at STC conditions.

The measurement data on the ac-power from the inverters were obtained from the monitoring device of the inverters themselves. These monitoring devices are not considered as accurate measurement instruments but the data serves as an indication of possible failures or sudden change in the performance of the PV-systems.

3.2 IV-tracer and spectrometer

In the course of the monitoring programme a number of shortlasting measurement campaigns were carried out. Besides standard laboratory equipment the following instruments were used for the measurement of the IV-curve of the arrays and for the measurement of the spectral distribution of the irradiance.

- IV-tracer: "I-V curve analyser for photovoltaics PV-KLA 4.3". Manufacturer Mencke & Tegtmeyer, Germany.
- Spectrometer: "Monolithic Miniature Spectrometer". Manufacturer Carl Zeiss, Germany.
Light collector: integrating sphere with a viewing angle of 2π sr.

4. SIMULATION TOOLS

The following simulation tools were applied:

- SPECTRL2 (<http://rredc.nrel.gov/solar>) for the calculation of the spectral distribution of the irradiance;
- PVcad1.2 (<http://www.iset.uni-kassel.de/abt/w3-a/pvcad>) for the calculation of shading effects;
- PVsyst3.1 (<http://www.unige.ch/gap-e/PVsyst/PVsyst.html>) for the calculations of various irradiation effects.
- ECN yield calculator (<http://www.ecn.nl/solar/yield>) for the calculation of annual energy production of PV-systems.

5. IRRADIATION

5.1 Data set

The monitoring system (paragraph 3.1) was used to collect data over a period of more than one year. The data were condensed into hourly values and were used to fill a data set of one year (365 days). Due to down time of the monitoring system a total of 0.7% of the year has no data. The monthly sums of the measured data are given in appendix 1 as obtained with the pyranometers and with the reference cells. The differences in the irradiation data from the pyranometers and the reference cells are caused by differences in the reflection and the spectral sensitivity. The effect of the reflection is addressed in paragraph 5.2 and the spectral effect is elaborated in paragraph 5.3. The data set was also used for the validation of models for the calculation of the diffuse irradiation (paragraph 5.4), of models for the calculation of irradiation on the tilted plane (paragraph 5.5) and of models for shading effects (paragraph 5.6).

5.2 Reflection

5.2.1 Introduction

The difference between the irradiation on the outer surface of the module and effectively on the solar cells is dependent on the incidence angle. Reference [1] gives the following expression for the ratio between the reflection at incidence angle θ and at normal incidence:

$K = 1 - b_0(1/\cos\theta - 1)$ in which K is called the “incidence angle modifier constant” and b_0 the “incidence angle modifier coefficient”. The ASHRAE-standard 93-77 suggests to use a b_0 value of 0.1 for a thermal solar collector with one glass cover. Reference [3] suggests to use a b_0 value of 0.05 for a PV-module. The value of K becomes negative at high values of θ (above 85° for $b_0 = 0.1$) which seems unrealistic. In reference [4] Sjerps-Koomen gives another reflection model in which K becomes zero at an incidence angle of 90° . The corresponding values of $K(\theta)$ are shown in figure 3.

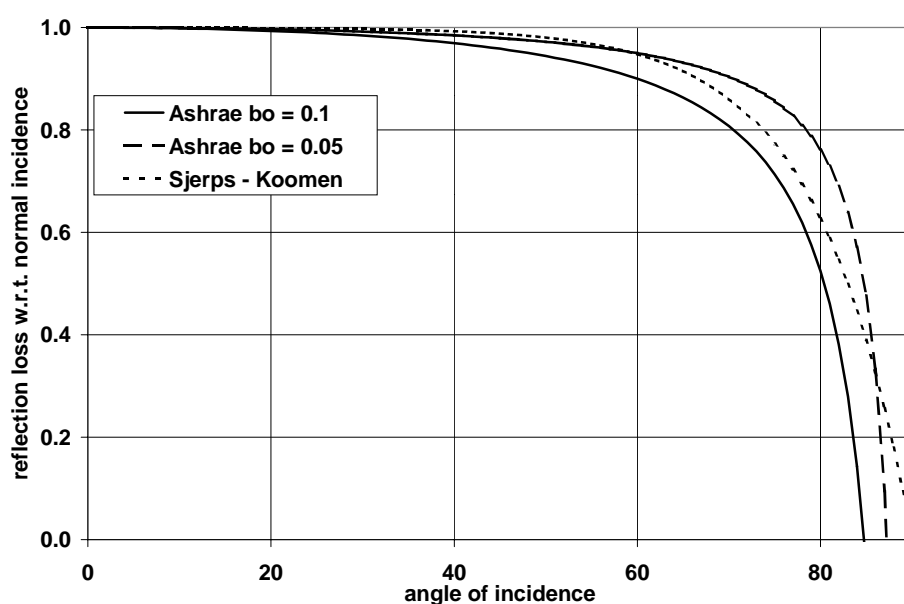


Figure 3: Reflection loss of a PV-module with respect to normal incidence

5.2.2 Model validation

The validation of the reflection model is based on the measured differences between a reference cell and a pyranometer, placed next to each other. It is assumed that the reflection effect on the modules is identical to the reflection effect on the reference cells on the façades. Furthermore it is assumed that the reflection effect of the pyranometers does not depend on the angle of incidence. Unfortunately the ratio between the measured data of the pyranometer and the reference cell is not only caused by the difference in reflection but also by the difference in the spectral response. The spectral effect is small around noon at April 1st and September 11th if the sky is clear since at those moments the irradiance spectrum is close to AM1.5 (see paragraph 5.2.3). On these moments the reflection effect is strong at the West façade because of the grazing incidence of the irradiance around noon. For these reasons the effect of reflection was studied using the measured data of the West façade on September 11th 2000 around noon (during which the sky was clear).

The pyranometer readings and the reference cell readings of the West façade were simulated with PVsyst, using the hourly measured irradiation (horizontal plane, total and diffuse) as input. The pyranometer readings were simulated using a K value of 1 and the reference cell readings were simulated using the K-values of figure 3.

The measured data on the West façade are given (as 10-minute averaged values) in figure 4 together with the calculated results (as mid-hourly data; PVsyst). The figure shows a somewhat better agreement with the measured data for the ASHRAE-model with $b_0 = 0.1$. However, the uncertainties of the calibrations of the reference cells and of the pyranometers (both estimated on 3% of the reading) make this choice almost arbitrary.

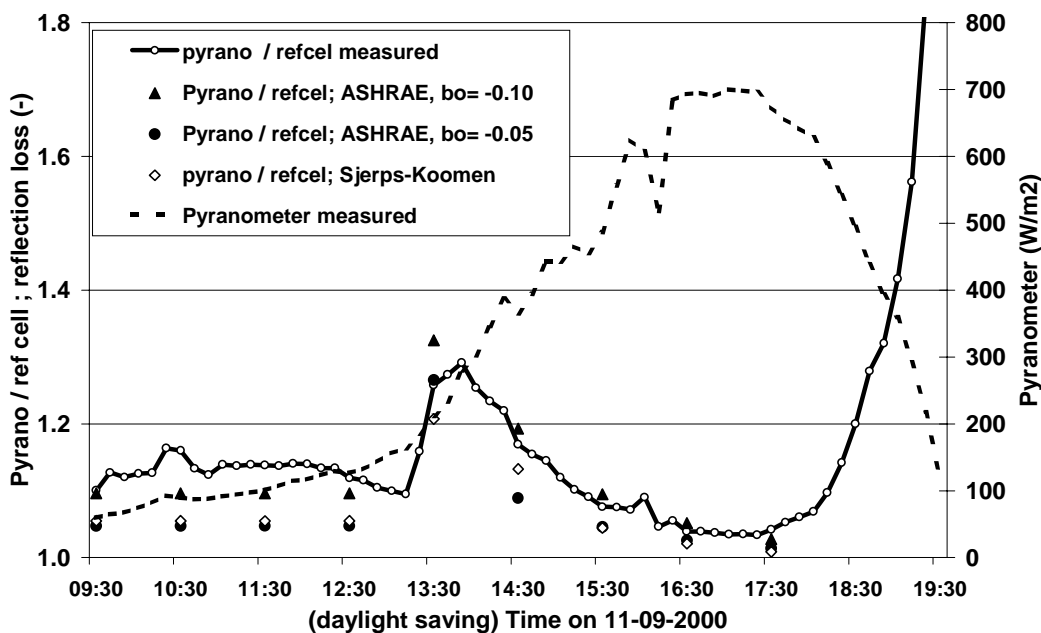


Figure 4: Pyranometer reading, ratio between pyranometer and reference cell reading and calculated reflection loss factor.

5.2.3 Quantification of the reflection loss

The reflection loss of the modules on the four facades were calculated by PVsyst using the ASHRAE-model with $b_0 = 0.1$ (simulating the reflection) and also with $b_0 = 0$ (simulating no reflection). The hourly measured irradiation (horizontal plane, total and diffuse) was used as input. The monthly reflection effects were calculated as the ratio of the monthly sums of the hourly output data. The results are shown in paragraph 5.3 (figure 8). This figure shows also the ratio between the monthly irradiations measured with the pyranometer and with the reference cell. The uncertainties in the readings of the reference cell and of the pyranometer are assumed to be uncorrelated and amount to 3 % each. This leads to the associated uncertainty of the measured ratios of 4%. This means that the difference between the pyranometer and reference cell reading on the South façade in the winter months and on the West façade in the non-summer months cannot fully be accounted for by the reflection losses. The remaining differences are attributed to the spectral effect (see paragraph 5.3).

The annual reflection losses were calculated as the ratio of the annual sums of the hourly output data of PVsyst. For comparison the annual reflection loss was also calculated in the same way for a module with optimal orientation in the Netherlands (exactly South with a tilt angle of 35°). This resulted in the following annual reflection losses.

	North facade	East facade	South facade	West facade	South; 35° tilt
Reflection loss factor	1.12	1.09	1.10	1.08	1.06
Pyranometer / ref. cell	1.11	1.06	1.09	1.13	not measured

Table 3: Calculated annual reflection loss factor and the measured ratio between the pyranometer and reference cell readings.

If the reflection loss for the West façade is calculated using the ASHRAE-model with $b_0 = 0.05$ or with the Sjerps-Koomen data the annual reflection loss factor amounts to 1.04 and 1.05 respectively. This shows that the calculated annual reflection loss factors in table 3 must be interpreted as upper estimates.

5.3 Spectral effect

5.3.1 Introduction

A solar cell has a wavelength-dependent response, meaning that its output is affected by the spectral distribution of the incident irradiance. The nominal power of a PV-module is normally defined for the standard irradiance spectrum: AM1.5. This is the solar spectrum as filtered by an air mass of 1.5 times the air mass when the sun is directly overhead.

In reality the modules are operated in spectra that deviate from the AM1.5 spectrum which can have a positive or a negative effect on the power output per unit irradiance. The spectral effect depends on the spectral response of the specific modules in question in combination with the spectral distribution of the irradiance.

5.3.2 Spectral response

The spectral response of amorphous silicon differs very much from that of crystalline silicon. Crystalline silicon is sensitive to wavelengths between 350 and 1200 nm and amorphous silicon is sensitive between 350 and 800 nm with a maximum sensitivity at 550 nm (reference [5]). In order to change the spectral response of the standard reference cells (made of crystalline silicon) to the spectral response of the amorphous silicon modules the reference cells were equipped with an optical filter (see paragraph 3.1).

The responses of the applied reference cells and of a mc-Si reference cell have been measured in the laboratory of ECN. The results are given in figure 5. Comparison with figure 1 of reference [5] shows that the applied reference cells have a spectral response that resembles that of amorphous silicon very well.

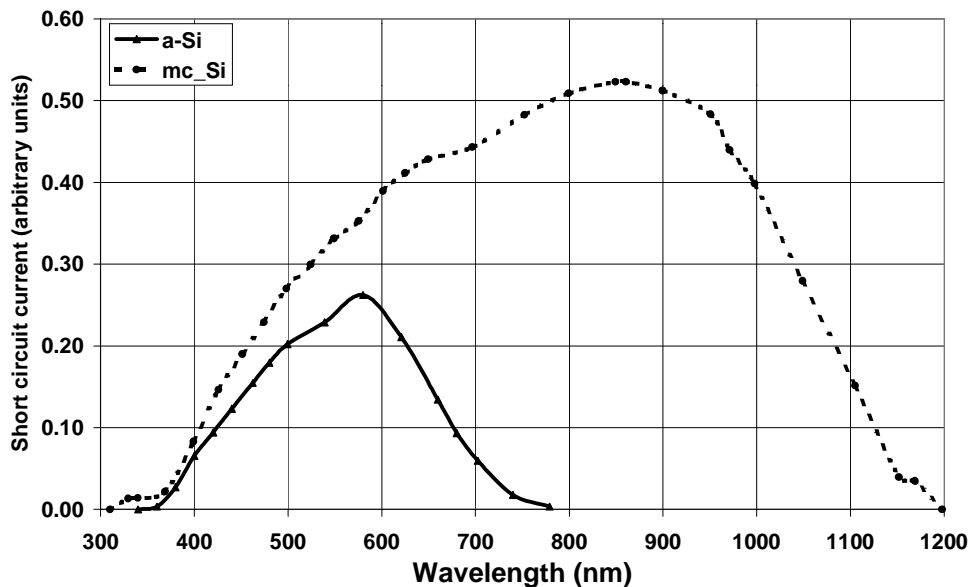


Figure 5: Spectral response of the "a-Si reference cell" and of a mc-Si reference cell, measured in the ECN laboratory.

5.3.3 Spectrum model

The spectral distribution of the irradiance on clear days (!) can be calculated with SPECTRL2. The output spectra of SPECTRL2 were checked with measurements performed during five measurement campaigns. The measurements resulted in relative spectra and covered the wavelength range of 300 nm to approximately 1000 nm. These spectra were normalised to the corresponding calculated spectra. The calculated spectra and the normalised measured spectra are shown in the appendix 8. The comparison of the calculated spectra with the measured spectra was only done for the roof, the South façade and the West façade. The calculated spectra for the North and East façade showed unrealistic values, probably caused by a negative angle of incidence of the direct beam on the North and East façades at the moment of the measurement campaigns. The output spectra of SPECTRL2 correspond rather well with the normalised measured spectra for the roof, South and West façade on clear days. In case of an overcast sky the measurements show significant differences with the calculations.

SPECTRL2 was used to calculate the spectrum on the West façade in the afternoon of 11-9-2000. On this day the sky was clear and at about 14.00h (local daylight saving time) the optical air mass is 1.5. The reading of the "a-Si reference cell" on the West façade was calculated by multiplying the calculated irradiance spectrum with the spectral response (figure 5). The reading of the pyranometer on the West façade was calculated by linear integration of the calculated irradiance spectra. The resulting ratios of the calculated pyranometer and reference cell reading,

normalised on the ratio of 14.00 h, are shown in figure 6. These results show a rather good correlation with the measured data.

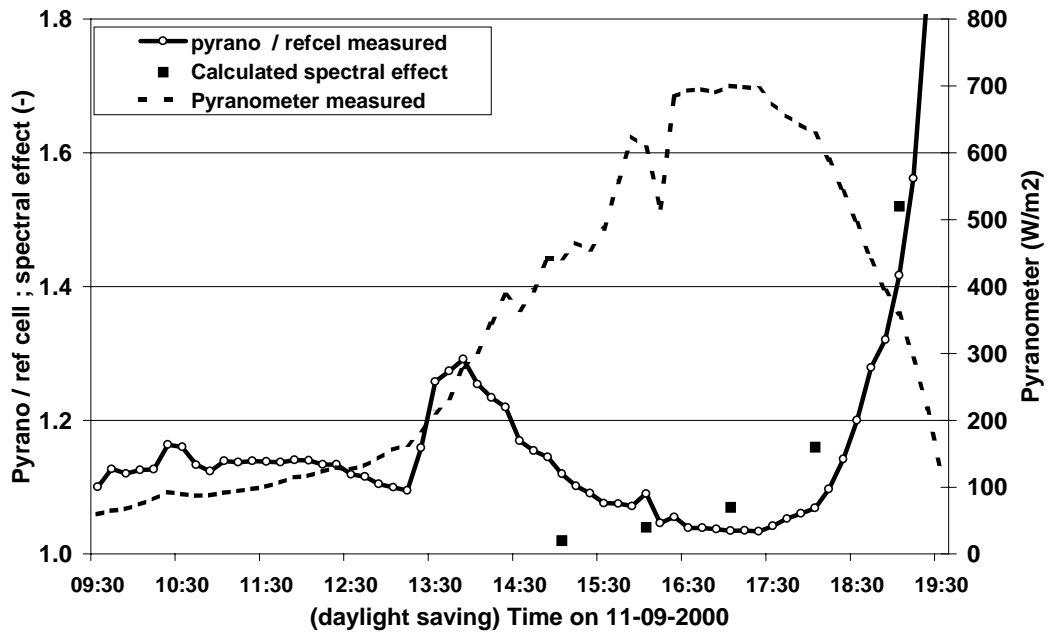


Figure 6: Pyranometer reading, ratio between pyranometer and reference cell reading and calculated spectral effect.

5.3.4 Quantification of the spectral effect

Figure 6 shows that a significant spectral effect occurs during the time of day that the irradiance on the West façade is significant. This is not the case for the North, East and the South façade (see figure 7). Consequently the energy loss caused by the spectral effect on the North, East and South façades are much smaller on that specific day.

The monthly and annual spectral effect cannot be calculated with SPECTRAL2 since this model is not developed for non-clear sky conditions. Therefore the monthly and annual spectral effect was determined per façade using the measured differences between the reference cell and pyranometer on that façade. The differences caused by the reflection losses were subtracted using the calculated reflection losses (paragraph 5.2.3). The remaining monthly differences, attributed to the spectral effect, are shown in figure 8. The annual differences, obtained from table 3, are given in table 4.

Spectral effect	North facade	East facade	South facade	West facade
	(-1 %)	(-3 %)	(-1 %)	5 %

Table 4: Estimate of the annual spectral effects; The values between brackets are too small in comparison with the measurement uncertainty for a reliable estimate.

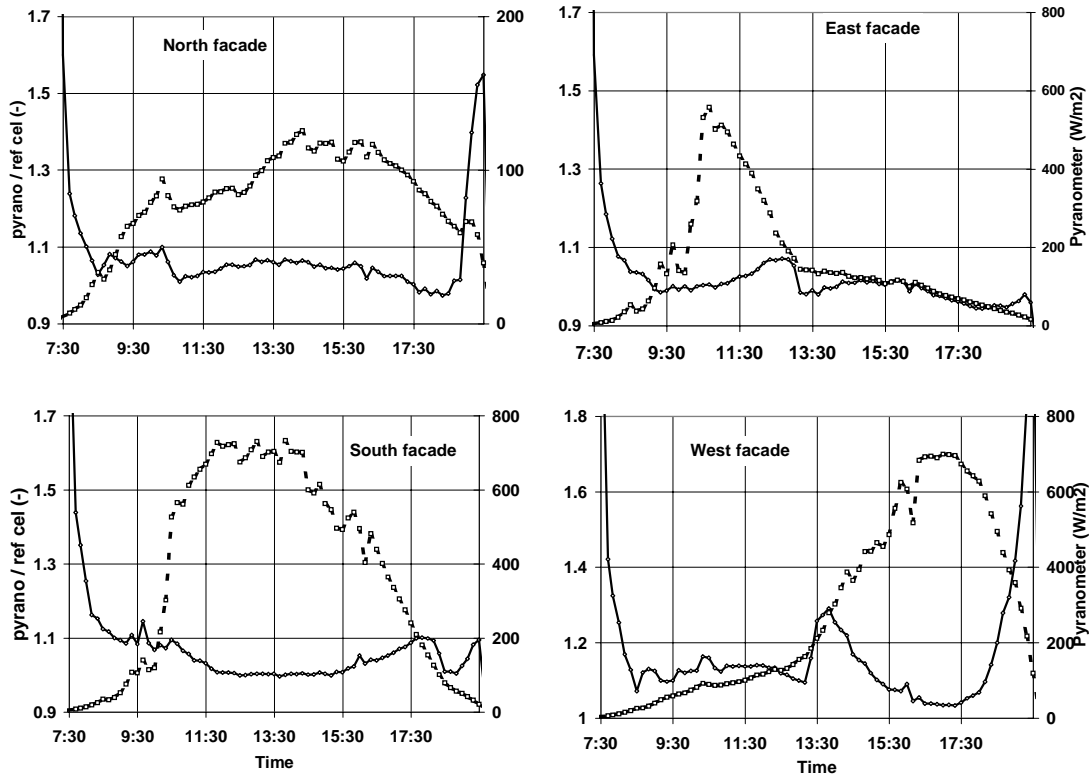


Figure 7: Pyranometer reading (dashed line) and ratio between pyranometer and reference cell reading (drawn line) on 11-09-2000.

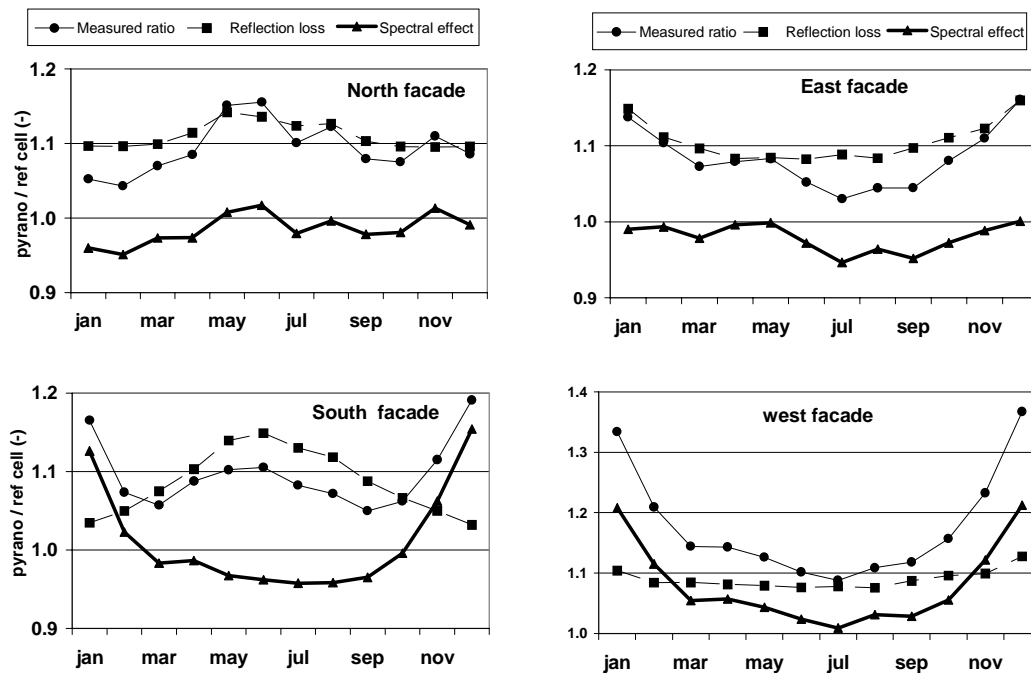


Figure 8: Measured ratio between the reading of the pyranometer and the reference cell, calculated reflection loss and the estimated spectral effect (remaining factor).

The estimated uncertainty in the ratio between the pyranometer and reference cell reading is 4% and the calculated reflection losses are regarded as upper estimates. Therefore the values of the spectral effects in figure 8 are only significant for the West façade during the non-summer

months and for the South façade during the winter months. The annual values of the spectral effect for the North, East and South façade are too small to be reliable. The value of the annual spectral effect of the West façade is regarded as an indication of the true spectral effect. The value is very much in line with the spectral effects for a-Si as given in the literature (references [6] and [7]).

5.4 Diffuse irradiation on the horizontal plane

5.4.1 Introduction

Very often only data on the global irradiation on the horizontal plane is available as input for the simulation tools, without data on its diffuse component. In these cases the diffuse component has to be calculated per time step using the measured global irradiation in combination with the solar position at the given location and moment. This can be performed with the Liu & Jordan model (1960) and also with the Orgill & Hollands model (1977) (see reference [1]). Both models are based on correlations between the diffuse fraction (defined as the hourly observed diffuse irradiation divided by the hourly observed global irradiation) and the clearness index (defined as the hourly observed global irradiation divided by the hourly calculated extraterrestrial irradiation at the given time and location). Both correlations are based on highly scattered data sets. Therefore the results of the models do not represent the diffuse fraction for a particular hour closely but over a long period of time the results should be reliable.

5.4.2 Model validation

Using the hourly values of the measured global irradiation on the roof of the building the hourly values of the diffuse irradiation on the roof of the building were calculated using the Liu & Jordan model and using the Orgill & Hollands model. The Liu & Jordan calculations were performed with PVSyst and the Orgill & Hollands calculations were performed with ZONsim. ZONsim is an undocumented program of ECN for internal use. The monthly and annual sums of the calculated diffuse irradiation values on the horizontal plane are compared with the measured data in figure 9. The measurement uncertainty in the reading of the pyranometers is estimated as 3 %. The discrepancies between the measured and calculated values of the monthly diffuse irradiation are much higher which means that the models are not very reliable on a monthly basis. The table shows that the Orgill & Hollands model performs somewhat better than the Liu & Jordan model. However for a complete year both models predict the diffuse irradiation without a significant discrepancy from the measured values.

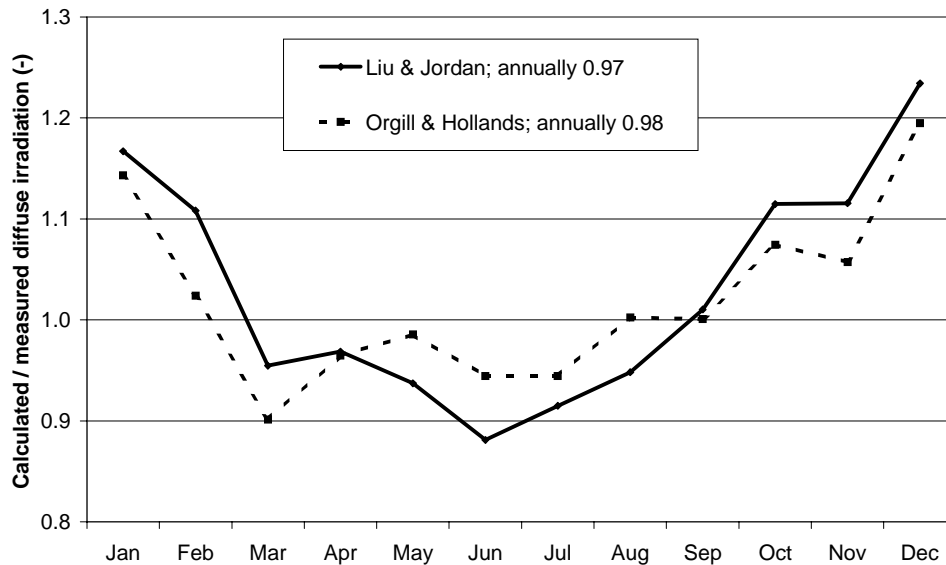


Figure 9: Ratio between calculated and measured diffuse component of the global irradiation

5.5 Irradiation on the tilted plane

5.5.1 Introduction

The irradiation on the tilted plane is composed of three components: the direct irradiation from the sun, the diffuse irradiation from the sky and the reflected irradiation from the surroundings (see reference [1]). The calculation of the irradiation on the tilted plane requires the global and the diffuse irradiation on the horizontal plane as input.

The calculation of the direct irradiation on the tilted plane is straightforward.

The calculation of the ground-reflected irradiation is relatively easy and requires only an estimated (or measured) reflection coefficient, called albedo. Some typical values for the albedo are 0.14 - 0.22 (urban situation), 0.15 - 0.25 (grass), 0.09 - 0.18 (asphalt) and 0.25 - 0.35 (concrete). A very commonly used value for the ground albedo is 0.2. The calculation of the irradiation caused by reflection of surrounding elements (such as buildings) can be very complicated.

The calculation of the diffuse irradiation on the tilted plane originating from the sky is far from straightforward. Perez (reference [2]) has modelled the diffuse component of the irradiation as the sum of the contributions from the circumsolar disc, the horizon area and the sky area. Hay & Davies (1980) neglected the contribution from the horizon area (see reference [1]). Both models were developed using on highly scattered data sets. Therefore the results of the models do not represent the irradiation on the tilted plane for a particular hour closely but over a long period of time the results should be reliable.

5.5.2 Model validation

The model of Perez and the model of Hay & Davies were validated by comparing the calculated irradiation on the tilted plane with the measured pyranometer readings. To make this validation as simple as possible only the data of the West façade was used since no shading obstacles are present there. The irradiation on the West façade was calculated using the measured pyranometer data on the roof (total and diffuse irradiation on the horizontal plane) as input with a value of the b_0 -parameter (see paragraph 5.2) of 0. The ground reflection coefficient (albedo) was set on 0.2.

The hourly values of the measured and calculated irradiation on the West façade are compared in figure 10. The measurement uncertainty in the reading of the pyranometers is estimated as 3

%. The discrepancies between the measured and calculated values of the monthly irradiation on the West façade are higher, especially in the winter months, which means that the models are not very reliable on a monthly basis. The figure shows that the Perez model performs better than the Hay & Davies model. For a complete year the Perez models predict the irradiation on the West façade without a significant discrepancy from the measured values. For this reason the Perez-model was used in the simulations of the following paragraphs.

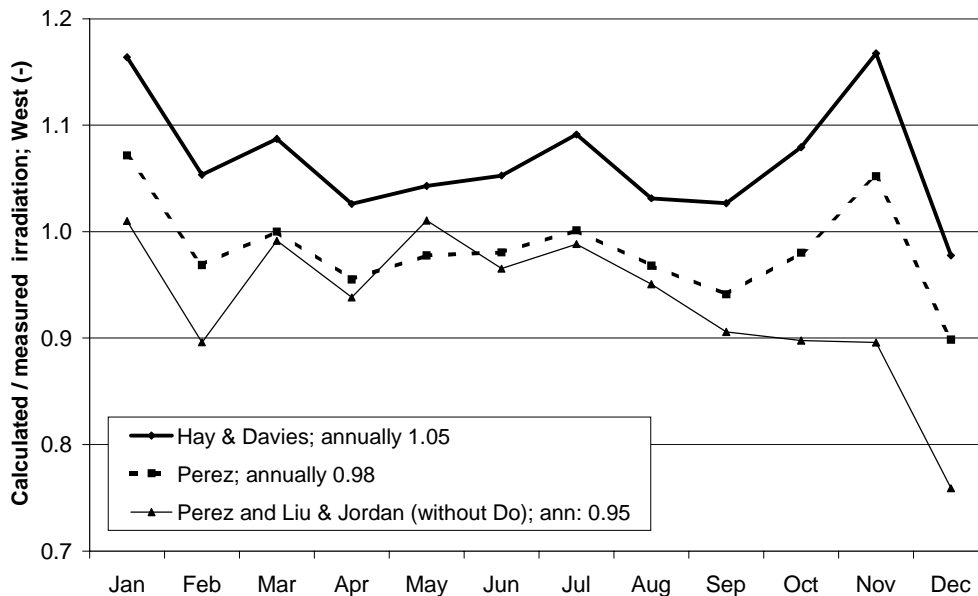


Figure 10: Ratio between the calculated and measured irradiation on the West facade.

The Perez model has also been validated in combination with the Liu & Jordan model (see paragraph 5.4.2) without the use of the measured values of the diffuse irradiation on the horizontal plane. The results (presented in figure 10) show, as expected, that the use of measured diffuse irradiation on the horizontal plane gives better data than the use of the synthesised values of the diffuse irradiation on the horizontal plane.

5.5.3 Orientation loss

The effect of orientation on the irradiation on the four façades without the influence of the shading neighbouring buildings was calculated with PVsyst. The irradiance on each façade was calculated using the measured pyranometer data on the roof (total and diffuse irradiation) as input with a value of the b_0 -parameter of 0 and an albedo of 0.2. The resulting annual irradiances are 304 (North), 525 (East), 830 (South) and 670 kWh/m² (West). For comparison also the irradiation on a plane with the optimal orientation for the Netherlands (South, 35 °) was calculated (1200 kWh/m²). Using these data the orientation loss of the four façades with respect to the optimal orientation in the Netherlands was calculated (see table 5)

North	East	South	West
75 %	56 %	31 %	44 %

Table 5: Orientation loss expressed in percents of the irradiation in the optimal situation (South, 35° tilt)

The irradiation on the West façade (with orientation 263 °, see table 1) is 28 % higher than the irradiation on the East façade (83 °). In case the West façade was exactly oriented towards West (270 °) and the East façade was exactly oriented towards East (90 °) the West façade would still receive 13 % more irradiation than the East façade. This "asymmetry" between East and West is probably influenced by the land/sea transition at the test location.

5.6 Shading

5.6.1 Introduction

Obstacles around a PV-system can reduce the various components of the irradiation on the tilted plane, mentioned in paragraph 5.5. The effect on the direct irradiation can be calculated in a straightforward way. The effect on the diffuse irradiation and on the surrounding-reflected irradiation is complicated. Two tools were used to calculate the total shading effects: PVsyst and Pvcad. PVsyst offers the user two methods for the shading calculations. These two methods are called “near shading” and “far shading”. In the “near shading” option the PV-system and its surroundings have to be defined 3-dimensionally. This enables PVsyst to calculate the irradiation on various points of the PV-system and consequently it enables PVsyst to account for mismatch effects due to partial shading. In the “far shading” option PVsyst sees the surroundings of the PV-system from one observation point only. In this option the elevation of the horizon has to be defined as a function of the azimuth angle. Both options are addressed in this paragraph. Since shading effects are time dependent, as is the reflection effect (paragraph 5.2), the shading and reflection effects are calculated simultaneously. PVsyst was used with a b_0 -value of 0 for comparison with measurement data from the pyranometers on the four façades and with a b_0 -value of 0.1 for comparison with the measurement data from the reference cells. The ground albedo was set on 0.2 for all simulations.

5.6.2 Near shading (PVsyst)

The near shading scene was defined for each of the four façades. The neighbouring buildings with a roof above the height of the irradiation sensors were defined as box-shaped elements (see figure 11). The results are compared with the measured data (see appendix 2). On annual basis the differences between the simulated and measured irradiation are between 8% (South) and 2% (West) for the pyranometer data. The comparison with the data from the reference cells shows almost identical results except for the West façade. The reference cell data from the West façade are biased due to the spectral effect during low solar position in the evenings (paragraph 5.3).

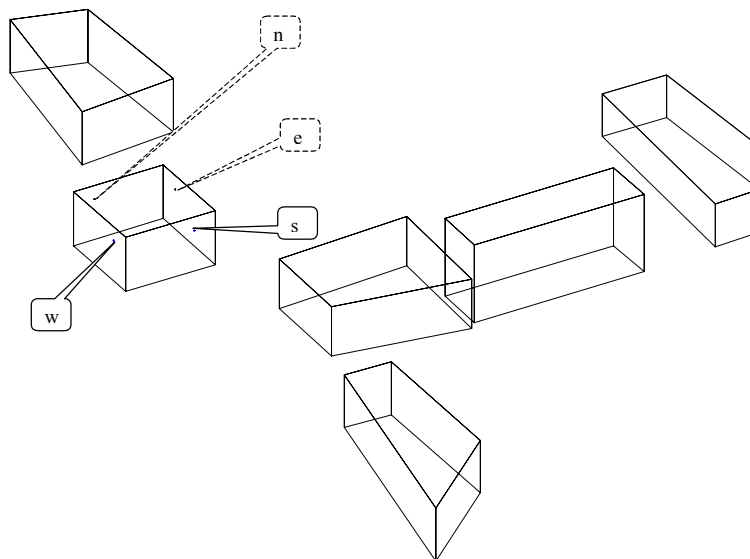


Figure 11: Near shading scene around the Renewable Energy Building

5.6.3 Far shading (PVsyst)

The horizon elevation caused by the neighbouring buildings was determined by calculations using the geometry of the near shading scene and was verified by measurements using a theodolite (see figure 12). PVsyst accounts for the effect of the elevated horizon on the direct radiation, on the diffuse radiation from the sky and on the diffuse radiation from the ground. Because the latter effect is ambiguous PVsyst offers the user a parameter (called “albedo fraction”) which acts as a reduction factor on the albedo-shielding. The “albedo fraction” (not to be mixed up with the albedo which was 0.2 throughout all simulations) was set on its minimum value (0%) and also on its maximum value (100%). The results of PVsyst with these two extreme values and with a b_0 -value of 0, was compared with the measured data from the pyranometers on the four façades in appendix 3. This appendix shows that the best agreement is reached using an “albedo fraction” of 100%. Seemingly the neighbouring buildings cause an augmentation of the irradiation (due to their diffuse reflection) that compensates more or less for their shielding-effect of the ground albedo.

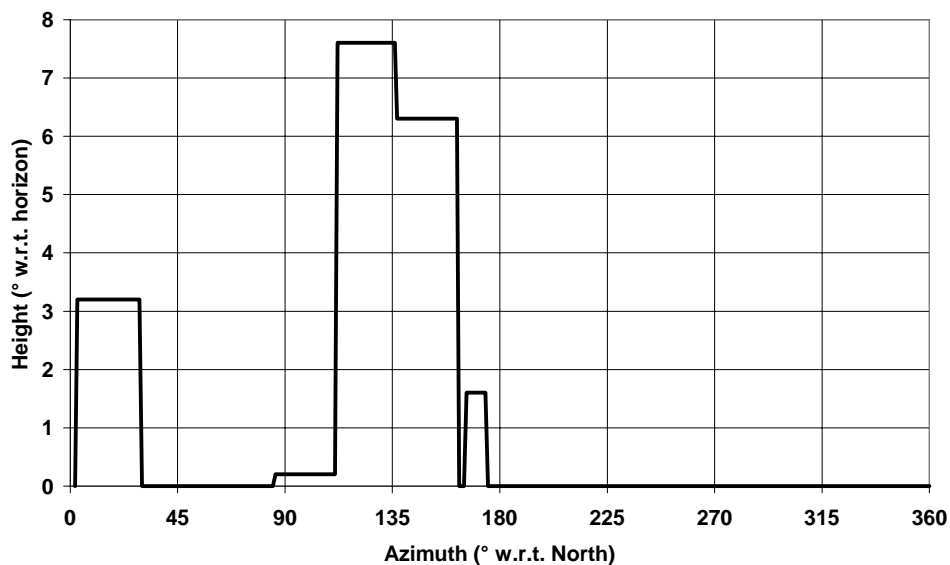


Figure 12: Far shading scene around the Renewable Energy Building

5.6.4 Near shading (PVcad)

PVcad was developed for the assessment of shadow effects in the built environment. It calculates the irradiance and temperature for each individual PV-module of the regarded PV-system using hourly data of the global and diffuse irradiation on the horizontal plane. PVcad accounts for the reflection effects of the modules. Unfortunately PVcad neglects the contribution of the ground reflection completely. For this reason it seems less opportune to validate PVcad in an absolute way using the measured data. As an alternative the shading factors were determined for each of the four façades by applying PVcad with and without the neighbouring buildings. The irradiation sensors and the neighbouring buildings were defined for PVcad using the programme AUTOCAD. Also PVsyst was used to calculate the irradiation on the façades with and without neighbouring buildings. This resulted in the shading factors for the near shading option and for the far shading option (with $b_0=0$ and albedo fraction = 100%). The results are given in appendix 4.

5.6.5 Discussion of the results

The data of appendix 4 are presented in the figure 13. Additionally this figure show the ratio between the simulated irradiances (PVsyst, far shading and near shading, with $b_0=0$ and albedo

fraction = 100%) and the measured irradiances (pyranometer). The differences between the simulated and measured irradiances on the West façade are only caused by uncertainties in measurement data from the pyranometers and in the model for converting the irradiation of the horizontal plane to the tilted plane. The effects of reflection and spectrum are not included since the data are obtained with the pyranometer and shading plays no role since the West façade is free of obstacles. This leads to the conclusion that the uncertainties in the measurements and in the tilt-model introduce an uncertainty in the ratio between measured and calculated monthly irradiances with an order of magnitude of 5% for an unshaded façade.

The deviations between the simulated and measured irradiances on the South façade however are significantly larger than this 5% during the summer months. This is discussed further in paragraph 5.7.2.

Figure 13 shows that the simulated shading factors are quite mild, meaning that the shading effects are small. Given the uncertainty in the ratio between measured and calculated monthly irradiances of about 5% the shading models cannot be validated accurately using the measured data. Only the data of the East façade during the months November, December and January show a significant simulated shading effect. Since the measured and simulated irradiances during these months on the East façade show only small differences it can be concluded that the shading models work satisfactory for these conditions.

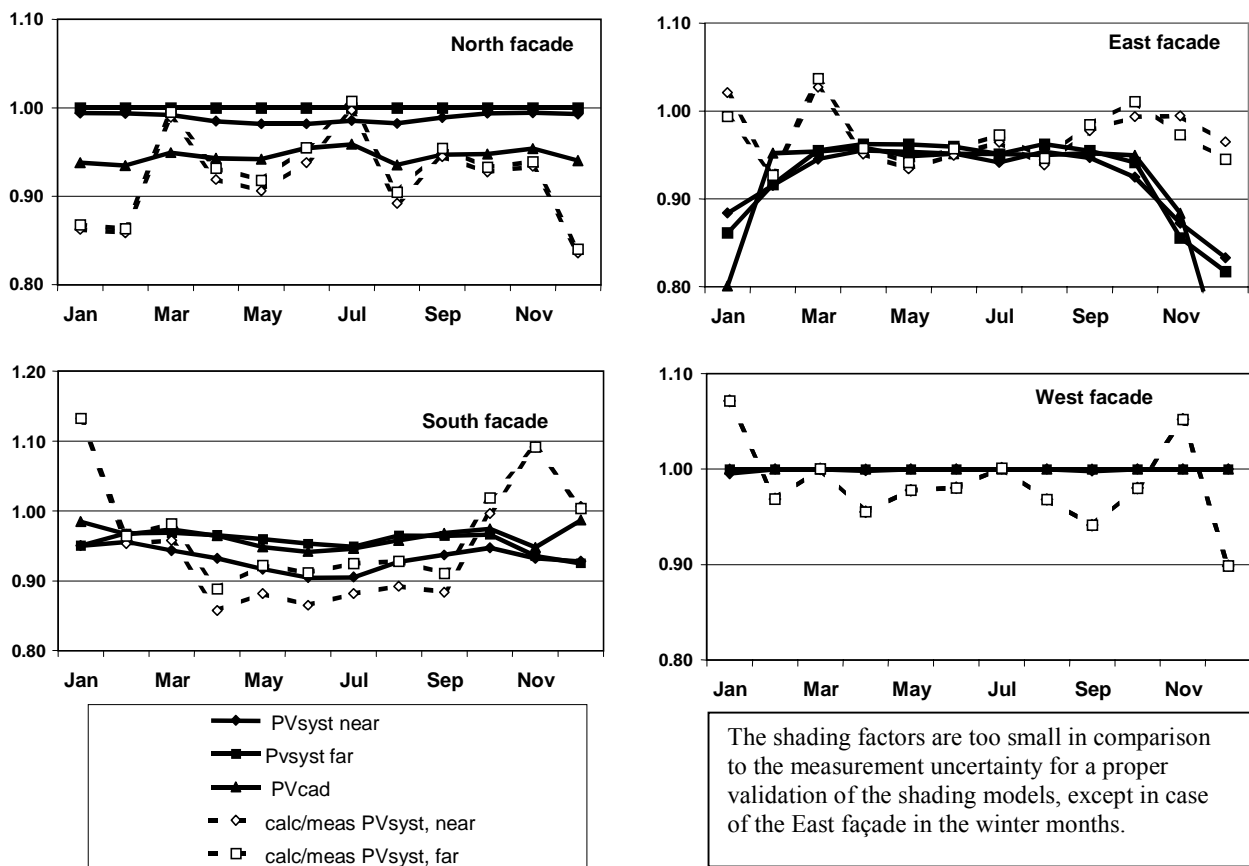


Figure 13: Calculated shading factors (drawn lines) and the ratio between calculated and measured irradiances (dashed lines)

The annual shading loss, calculated with the near shading model of PVsyst, is given in table 6.

North	East	South	West
1 %	6 %	7 %	0 %

Table 6: Annual shading loss (PVsyst, near shading)

5.7 Observations concerning PVsyst

5.7.1 Perez model

Although the results of the Perez model seems to be in line with the measured data on the West façade (see paragraph 5.5.2) the results for the South façade is somewhat disappointing (see paragraph 5.6.5). For finding the reason of this discrepancy the Perez-model was also programmed in an ad-hoc programme of ECN.

Running PVsyst and the ECN programme without shading and both with the same input data resulted in remarkable differences. The beam contribution and the ground reflected contribution to the irradiation on the facades are more or less identical for both programmes. The contribution from the diffuse sky however showed significant differences for the East, South and West facades. This observation was communicated with the developer of PVsyst. The developer concluded that PVsyst did not exactly follow the Perez model.

However the influence of the mistake in PVsyst is relatively small and therefore the consequences for the results of chapter 5 are limited. Nevertheless, further modelling (chapter 7) is performed with another tool.

5.7.2 Ground reflection

It was noted that the annual contribution of the ground reflected irradiation towards the facades was not calculated by PVsyst as expected. Scrutinising the hourly output data of PVsyst showed that the ground reflection was programmed in a special way.

The description of the applied model for the ground reflection, given in the "help-function" of PVsyst is in compliance with the model of reference [1]. In this model the ground reflected irradiation is calculated from the global irradiation on the horizontal plane. However the actual calculation of the ground reflected irradiation by PVsyst is based upon the following.

- When the sun is behind the module the ground reflection is calculated from the diffuse irradiation on the horizontal plane,
- when the sun is not behind the module the ground reflection is calculated from the global irradiation on the horizontal plane.

Although this calculation method is not according to the documentation of PVsyst, it is not necessarily incorrect. In case the array is very large the ground in front of the modules receives the diffuse irradiation when the sun is behind the modules. In case the array is small the ground in front of the modules receives the global irradiation when the sun is behind the modules. This means that for very large arrays the PVsyst calculation method might be a better approach than the standard method.

The difference between the PVsyst method and the standard method for the calculation of the ground reflected irradiation towards the tilted plane depends very much on the orientation of the modules. The PVsyst method results in a 0.4% lower irradiance on the South façade than the standard method. However the PVsyst method results in a 16% lower irradiance on the North façade than the standard method.

6. TEMPERATURES

The temperatures of the modules, of the air gap behind the modules, of the wall behind the modules and of the wall next to the modules were measured on the South and West façade. The measurement data were segregated into data obtained at low wind speed (< 6 m/s) and at high wind speed (> 8 m/s). The differences of the temperatures with the ambient temperature were averaged in intervals of irradiance (bins) with a width of 50 W/m^2 . The results are presented in figure 14. The figure shows that the wall behind the modules remains significantly cooler than the wall next to the modules. The temperature of the air gap behind the modules remains much lower than of the modules. This shows that the modules are relatively well ventilated. The measured temperature increase of the modules with respect to the ambient temperatures per unit irradiance (the so-called k-factor) is given in table 7.

Wind speed range (m/s)	k (West) (K/W/m ²)	k (South) (K/W/m ²)
< 6	0.032	0.031
> 8	0.023	0.022
all	0.030	0.026

Table 7: Temperature increase of the modules with respect to the ambient temperatures per unit irradiance.

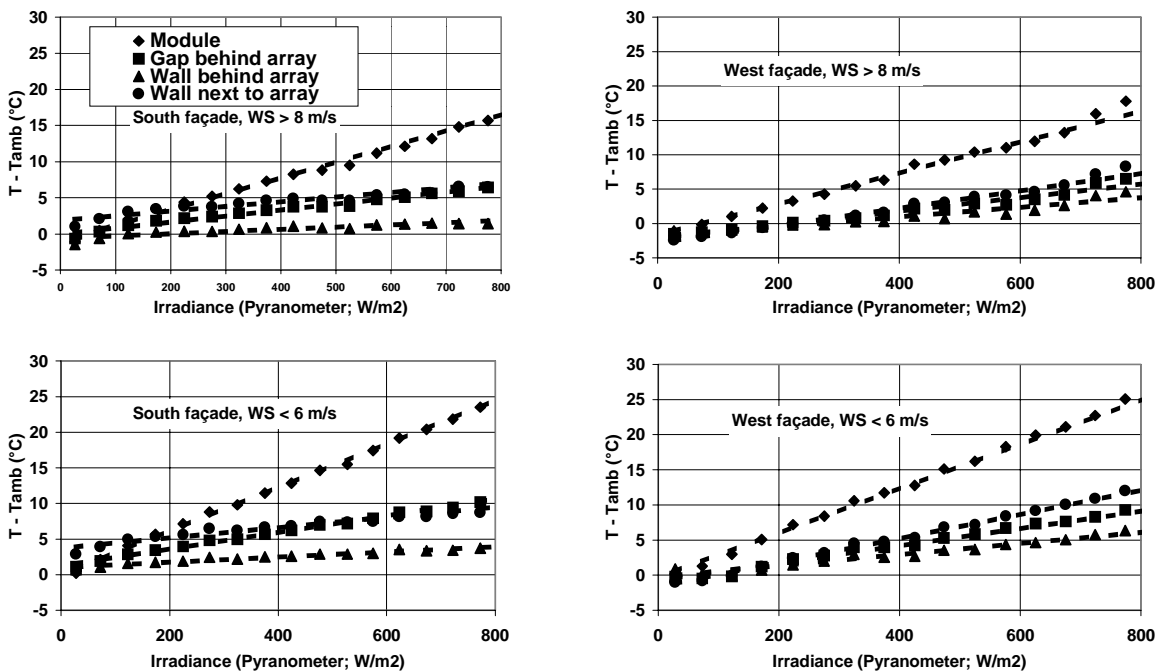


Figure 14: Measured temperature differences with respect to the ambient temperature

The temperature coefficient of the module power at the maximum power point is very small (reference [8], table 4). For this reason the effect of the module temperature on the annual energy production was not assessed.

7. ENERGY PRODUCTION

7.1 Measurements

The energy production of the four PV-systems was determined using the data as measured with the monitoring system. Unfortunately this monitoring system provides no reliable information on the energy production directly. As an alternative the energy data of each of the four PV-systems were synthesised on a 10-minutes basis using the irradiance data as measured with the reference cells. For each 10-minutes period the array output was calculated by multiplication of the irradiance (measured with the "a-Si reference cells") with the corresponding array efficiency. For each 10-minutes period the inverter output was calculated by multiplication of the array output with the corresponding inverter efficiency. This requires the use of an efficiency curve of the arrays and an efficiency curve of the inverters. Both curves have been measured.

Array efficiency.

The efficiency of the array on the South façade was determined by measuring its IV-curve at various values of the irradiance. The irradiance was measured using the reference cell of the monitoring system. Each performed IV-curve measurement resulted in an array power value at the maximum power point. Using these data in combination with the measured irradiance and the effective cell area ($42 * 0.264 = 11.09 \text{ m}^2$) the efficiency curve of the South array were determined as shown in figure 15. The data of the figure were used as the efficiency curve for each of the four arrays. This means that possible time effects were ignored as well as possible differences between the efficiencies of the four arrays. Furthermore it is assumed that the arrays are always operated in their maximum power point.

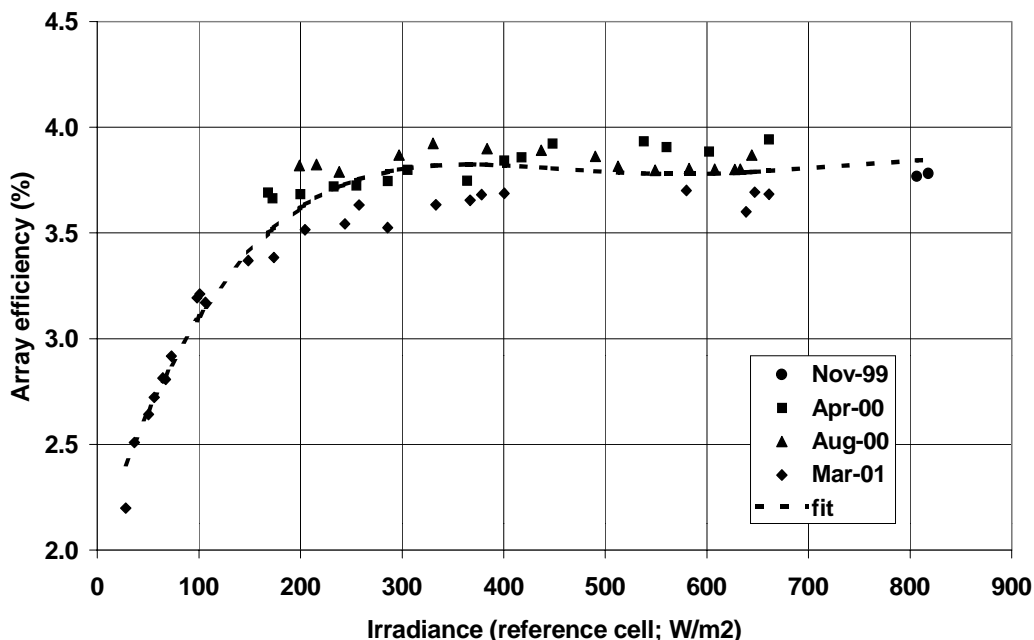


Figure 15: Array-efficiency, based on the effective cell area, of the South array as obtained by IV-curve measurements. The dashed line is an eye guide. The estimated uncertainty of the values is 5 %.

Inverter efficiency.

The conversion efficiency of a SunnyBoy 700 inverter was measured in the laboratory at various values of the input power. The power measurements were performed using a power analyser (NORMA D6000). The range of the input voltage was set on 75 - 150 V. The measured conversion efficiency is given in figure 16. The line in the figure was used to account for the conversion loss in the inverter of each of the four PV-systems.

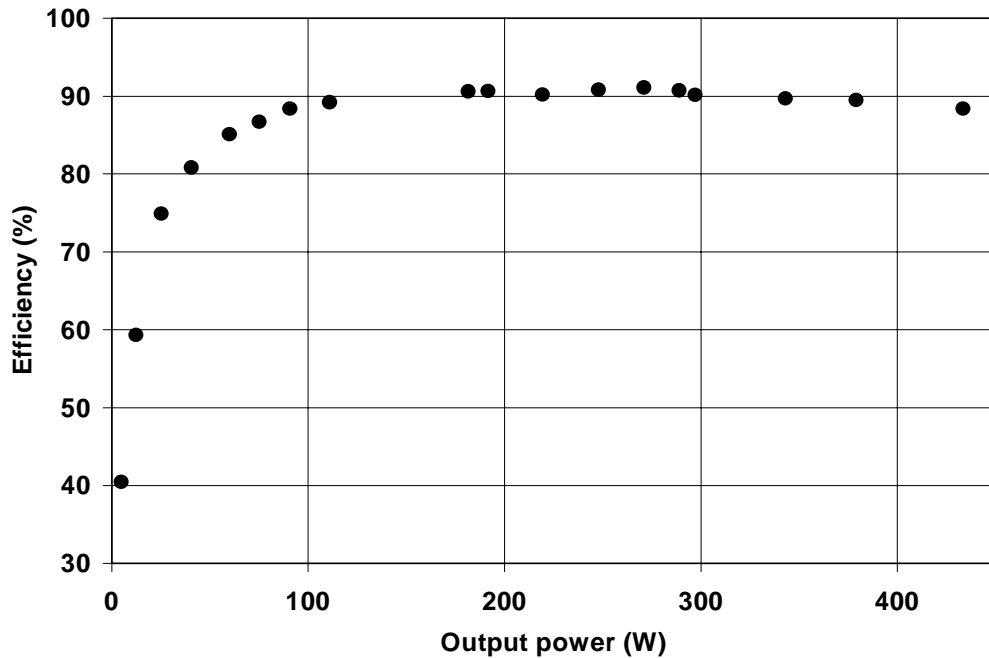


Figure 16: Conversion efficiency of a SunnyBoy 700 inverter, measured in the laboratory. Settings: input voltage range 75 - 150 V; input power range: 0 - 420 W. The estimated uncertainty of the values is smaller than 1 %.

The monthly averaged values of the synthesised power values were multiplied by the duration of the corresponding months. This resulted in the monthly energy values as given in appendix 5. With the data of this appendix the monthly values of the array efficiencies and of the inverter efficiencies were calculated (see appendix 6). Appendix 6 shows that the annual array efficiencies are lower than the optimal value of 3.8 % (see figure 14). This is caused by the contribution of the irradiation at low irradiance values which is different for the various façades (see figure 17). Taking 3.8% as a reference the following values for the low irradiance loss were calculated from the annual data of appendix 6.

North	East	South	West
20 %	10 %	5 %	7 %

Table 8: Annual low irradiance loss

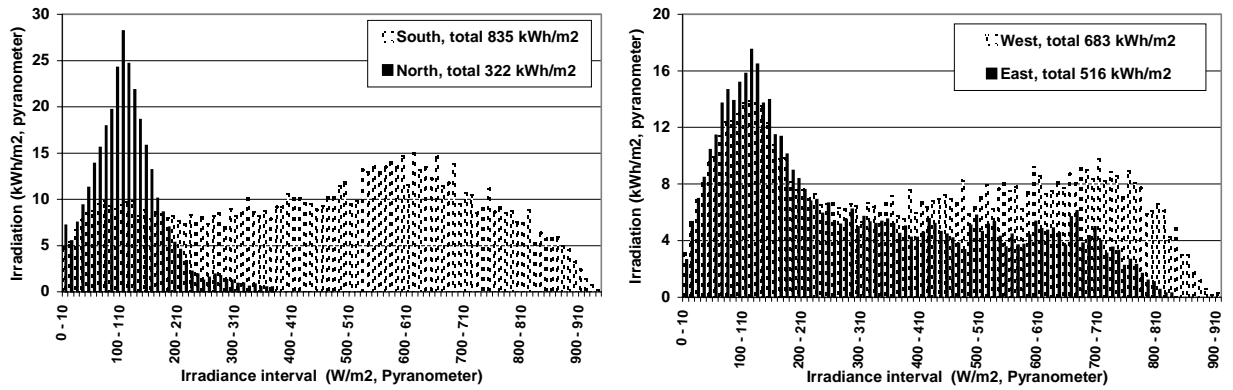


Figure 17: Annual frequency distribution of the irradiation.

From appendix 6 the following values are obtained for the annual inverter loss.

North	East	South	West
32 %	20 %	14 %	17 %

Table 9: Annual inverter loss

Table 9 shows that the annual inverter loss of the North system is much higher than that of the South system. This extra energy loss could be avoided by selecting an inverter with a nominal power that matches with the expected maximum power instead of the nominal power of the North façade.

Appendix 7 shows the monthly performance ratio's and the annual yield values. These data are based on the nominal power of the modules ($12 W_p$). The annual performance indicators of appendix 7 are repeated in table 10.

	North	East	South	West
Performance ratio (-)	0.46	0.61	0.68	0.65
Yield (kWh/kW _p)	132	291	526	388
Yield (kWh/kW _p), normalised to 1000 kWh/m ² global irradiation	126	277	499	369

Table 10: Annual performance indicators, based on the nominal power of $12 W_p$ per module. Since the actual power of the modules are about $10 W_p$ the values are biased in a negative way.

7.2 Performance modelling

The output of each of the four PV-systems was modelled using the ECN Yield programme. The calculation of the irradiation on the tilted plane is performed using the Perez-model (see paragraph 5.5).

The albedo effect was calculated using the PVsyst method (see paragraph 5.7.2) and an albedo value of 0.2.

The reflection loss on the front cover of the modules is based on the Sjerps-Koomen model (see paragraph 5.2).

The array output is calculated using the measured DC-efficiency curve and the inverter output is calculated using the measured conversion efficiency curve.

The calculations are performed in hourly steps.

The input for the calculations were the following:

- geographical position, azimuth and tilt angles of the arrays (see paragraph 2),
- hourly values of the global and diffuse irradiation, measured on the roof of the building (see paragraph 5.1),
- measured array efficiency curve (dashed line in figure 15),
- inverter efficiency curve of the Sunny Boy 700 from the library in the programme (almost identical to the data in figure 16).

The temperature effect has not been taken into account (see last line of paragraph 6). The programme does not account for shading and for the spectral effect. The shading effect has been applied on the annual output data of the programme (taken from table 6). The spectral effect has also been applied on the annual output data of the programme (taken from the measured difference between pyranometer and reference cell, table 3, minus the reflection loss calculated by the ECN Yield programme). The spectral effect was not applied for the North, East and South façade since the value of the spectral effect was insignificant in comparison to the measurement uncertainty.

The annual results of the performance calculations are given in table 11 (irradiation), 12 (array output) and 13 (inverter output). These tables show also the measured data (last line of appendix 5).

Table 11 shows that the modelled irradiation on the solar cells is within 6 % of the measured values. The results in table 11 are more or less reflected in the data of tables 12 and 13. The low value of the calculated irradiation on the North façade is amplified in the tables 12 and 13 because of the low irradiance loss in the modules and because of the partial load loss in the inverter respectively.

	North façade	East façade	South façade	West façade
Irradiation (kWh/m ²)	299	545	912	715
Reflection loss (%)	8	6	5	5
Spectral effect (%)	(3)	(0)	(4)	8
Shading loss (%)	1	6	7	0
Calculated resulting irradiation (kWh/m ²)	272	482	806	625
Measured irradiation (kWh/m ²)	289	481	770	601
Calculated / Measured irradiation (-)	0.94	1.00	1.05	1.04

Table 11: Modelled and measured irradiation, effectively available for the a-Si cells.

	North façade	East façade	South façade	West façade
Array output (kWh)	91	195	348	267
Spectral effect (%); see table 11	(3)	(0)	(4)	8
Shading loss (%)	1	6	7	0
Calculated resulting output (kWh)	90	185	324	246
Measured array output (kWh)	98	183	309	235
Calculated / Measured output (-)	0.92	1.01	1.05	1.05

Table 12: Modelled and measured array output.

	North façade	East façade	South façade	West façade
Inverter output (kWh)	61	158	303	226
Spectral effect (%); see table 11	(3)	(0)	(4)	8
Shading loss (%)	1	6	7	0
Calculated resulting output (kWh)	60	149	282	208
Measured inverter output (kWh)	67	147	265	196
Calculated / Measured output (-)	0.90	1.01	1.06	1.06

Table 13: Modelled and measured inverter output.

8. SYSTEM RELIABILITY

The reliability of the four PV-systems was observed in the following way.

- Visual inspection of the modules.
- Evaluation of the inverter output power, obtained with the monitoring facility of the inverters, in relation to the irradiance, obtained with the reference cells

Visual inspection of the modules showed a beginning delamination in some of the modules in November 2000. The delamination of one of the modules (of the East façade) was caused by a crack in the glass, probably initiated during the mounting. An example of the delamination of one of the modules of the North façade is given in figure 18 (picture of 21/05/2001).



Figure 18: Delamination of a module on the North façade.

The evaluation of the power data from the monitoring facility of the inverters resulted in monthly curves of the system efficiency versus the irradiance. Since the monitoring facility is not considered as reliable measurement equipment, these curves are not presented in this document. However the monthly evaluation of the efficiency curves values gave no indication of a deterioration of any of the four PV-systems up to the end of the monitoring period (August 2001). Apparently the beginning delamination of the modules causes no significant loss of performance.

9. CONCLUSIONS

General

- Reflection effects due to non-normal incidence are significant and can be accounted for using available simulation tools.
- Spectral effects of a-Si modules are significant but the used simulation tools have no possibility to determine its annual effect.
- Synthesis of the diffuse irradiation on the horizontal plane using measured data of global irradiation can be performed using the model of Liu & Jordan and the model of Orgill & Hollands. The latter performs somewhat better. The model output on monthly basis is not very reliable but on annual basis the results are correct.
- Total irradiation on the tilted plane using total and diffuse irradiation on the horizontal plane can be calculated using the models of Hay & Davies and of Perez. The model output on monthly basis is not very reliable but on annual basis the results are correct.
- The three examined shading models (near shading and far shading of PVsyst and near shading of PVcad) show significant differences.

Specific

- The measured temperature increase of the modules with respect to the ambient temperatures per unit irradiance is 0.031 K/W/m^2 at low wind speeds ($< 6 \text{ m/s}$). At high wind speeds ($> 8 \text{ m/s}$) the measured value amounts to 0.023 K/W/m^2 .
- The annual energy loss in the DC/AC conversion is relatively high for the PV-system of the North façade due to the partial load losses. The partial load losses could be decreased by a more appropriate inverter selection, based upon the frequency distribution of the array power rather than based upon the nominal array power.
- The inverters have worked without any breakdown during the complete monitoring period.
- The modules show a beginning delamination after an operation period of about 24 months.
- The most important annual energy data are summarised in the following table.

	see	North façade	East façade	South façade	West façade
Azimuth angle		353°	83°	173°	263°
Orientation loss (%); with respect to South, 35°	par. 5.5.3	75	56	31	44
Estimated shading loss (%); PVsyst, near shading	par. 5.6.5	1	6	7	0
Reflection loss (%)	par. 7.2	8	6	5	5
Spectral loss (%); Estimation	par. 7.2	?	?	?	8
Low irradiance loss (%); reference value $\eta_{\text{module}} = 3.8 \%$	par. 7.1	20	10	5	7
Inverter loss (%); DC / AC conversion	par. 7.1	32	20	14	17
Performance ratio (-); reference: $P_{\text{stc}} = 42 \cdot 12 W_p$; H_i measured with reference cells	par. 7.1	0.46	0.61	0.68	0.65
Yield (kWh/kWp); reference: $P_{\text{stc}} = 42 \cdot 12 W_p$; H_0 measured with pyranometer	par. 7.1	132	291	526	388
Normalised Yield (kWh/kWp); normalised to $H_0 = 1000 \text{ kWh/m}^2$	par. 7.1	126	277	499	369

The following observations are made concerning this table:

1. The spectral losses are not presented for the North, East and South façades because the loss values are too small in comparison with the measurement uncertainty for a reliable estimate.
2. The differences in the low irradiance losses are caused by the differences in the frequency distributions of the irradiation on the four arrays.
3. The differences in the inverter losses are caused by the differences in the frequency distributions of the array power from the four arrays and consequently by the differences in the partial load losses in the inverters.
4. The values of the performance indicators (performance ratio, yield, normalised yield) are biased in a negative way because of the used nominal power of $12 W_p$. The actual power of the modules was about $10 W_p$ ($\eta_{\text{module}} = 3.8 \%$ based on an effective cell area of 0.264 m^2).

10. REFERENCES

- [1] J.A. Duffie, W.A. Beckmann: "Solar engineering of thermal processes" 2nd edition (1991); ISBN 0-471-51056-4.
- [2] R. Perez, P. Ineichen, R. Seals, J. Minalsky, R. Stewart: "Modeling daylight availability and irradiance component from direct and global irradiance" Solar Energy 44, no 5, pp 271 - 289, 1990.
- [3] P. Schaub, A. Mermoud, O. Guisan: "Evaluation of the different losses in two photovoltaic systems"; 12th European PV solar energy conference, Amsterdam, 11-15 April 1994.
- [4] E.A. Sjerps-Koomen, E.A. Alsema: "A model for PV module reflection losses under field conditions"; 13th European PV solar energy conference, Nice, 23-27 October 1995.
- [5] J. Metzdorf, S. Winter, T. Wittchen: "Radiometry in photovoltaics; calibration of reference solar cells and evaluation of reference values"; Metrologica, 2000, 37, p573 - p578.
- [6] C.J. Riordan, R.L. Hulstrom: "Summary of studies that examine the effects of spectral solar radiation variations on PV device design and performance"; SERI/TR-215-3437; Golden (Colorado), March 1989.
- [7] S. Nann: "Variabilität der spectrale Bestrahlungsstärke der Sonneneinstrahlung und deren Einfluß auf den Wirkungsgrad von Solarzellen", Oldenburg University, Oldenburg 1992.
- [8] J.A. Eikelboom, M.J. Jansen: "Characterisation of PV modules of a new generation"; ECN-C-00-067; Petten, June 2000.

APPENDICES

Appendix 1: Measured irradiation values per month

Month	horizontal, pyranometer (kWh/m ²)		vertical, pyranometer (kWh/m ²)				vertical, reference cell / pyranometer (-)				MF
	Diffuse	Global	East	North	South	West	East	North	South	West	
Jan	13.2	23.5	12.2	7.8	43.8	19.5	0.88	0.95	0.86	0.75	1.00
Feb	21.6	42.0	23.1	12.6	65.9	33.0	0.91	0.96	0.93	0.83	1.00
Mar	43.4	71.3	33.6	21.6	69.4	46.0	0.93	0.93	0.95	0.87	1.00
Apr	52.7	105.7	58.3	29.8	87.6	64.9	0.93	0.92	0.92	0.87	0.97
May	70.4	165.3	80.3	47.2	100.4	101.2	0.92	0.87	0.91	0.89	0.97
Jun	83.8	181.8	85.3	58.0	94.8	112.0	0.95	0.87	0.90	0.91	1.00
Jul	83.4	139.8	64.0	47.8	76.3	85.5	0.97	0.91	0.92	0.92	1.00
Aug	69.9	162.3	79.8	42.9	115.2	104.1	0.96	0.89	0.93	0.90	1.00
Sep	48.0	81.4	39.8	25.2	73.9	53.8	0.96	0.93	0.95	0.89	1.00
Oct	25.8	41.8	19.8	14.0	44.8	30.3	0.93	0.93	0.94	0.86	1.00
Nov	13.9	19.4	9.5	7.6	23.9	14.7	0.90	0.90	0.90	0.81	1.00
Dec	11.0	17.6	9.8	6.8	37.1	16.5	0.86	0.92	0.84	0.73	1.00
Total	538	1054	516	322	835	683	0.94	0.90	0.92	0.88	0.99

MF = monitoring time-fraction

Appendix 2: Comparison between simulated (PVsyst, near shading) and measured irradiances (pyranometers and reference cells).

Period	PVsyst (b ₀ =0) / measured (pyrano)				PVsyst (b ₀ =0.1) / measured (ref cel)			
	North	East	South	West	North	East	South	West
January	0.86	1.02	1.13	1.07	0.83	1.01	1.28	1.31
February	0.86	0.93	0.95	0.97	0.82	0.92	0.98	1.08
March	0.99	1.03	0.96	1.00	0.97	1.01	0.94	1.06
April	0.92	0.95	0.86	0.96	0.91	0.95	0.85	1.02
May	0.91	0.93	0.88	0.98	0.93	0.94	0.86	1.03
June	0.94	0.95	0.87	0.98	0.97	0.93	0.84	1.01
July	1.00	0.96	0.88	1.00	0.99	0.92	0.85	1.01
August	0.89	0.94	0.89	0.97	0.90	0.91	0.86	1.00
September	0.94	0.98	0.88	0.94	0.93	0.94	0.86	0.98
October	0.93	0.99	1.00	0.98	0.92	0.97	1.00	1.03
November	0.93	0.99	1.09	1.05	0.95	0.99	1.16	1.18
December	0.84	0.96	1.01	0.90	0.83	0.97	1.16	1.10
Annual	0.93	0.96	0.92	0.98	0.93	0.94	0.92	1.03

Appendix 3: Comparison between measured (pyranometer) and simulated irradiations. The simulations were performed with PVsyst (far shading) using the two extreme values of the albedo fraction (not to be mixed up with the albedo which was 0.2).

Period	PVsyst ($b_0=0$) / measured (pyrano)							
	Albedo fraction 0%				albedo fraction 100%			
	North	East	South	West	North	East	South	West
January	0.87	0.87	1.08	1.07	0.87	0.99	1.13	1.07
February	0.86	0.80	0.91	0.97	0.86	0.93	0.96	0.97
March	1.00	0.89	0.89	1.00	1.00	1.04	0.98	1.00
April	0.93	0.84	0.78	0.96	0.93	0.96	0.89	0.96
May	0.92	0.82	0.79	0.98	0.92	0.94	0.92	0.98
June	0.95	0.83	0.75	0.98	0.95	0.96	0.91	0.98
July	1.01	0.82	0.77	1.00	1.01	0.97	0.92	1.00
August	0.90	0.83	0.81	0.97	0.90	0.95	0.93	0.97
September	0.95	0.85	0.81	0.94	0.95	0.98	0.91	0.94
October	0.93	0.87	0.94	0.98	0.93	1.01	1.02	0.98
November	0.94	0.83	1.02	1.05	0.94	0.97	1.09	1.05
December	0.84	0.82	0.96	0.90	0.84	0.95	1.00	0.90
Annual	0.94	0.83	0.84	0.98	0.94	0.96	0.95	0.98

Appendix 4: Shading factors calculated with PVsyst (far shading and near shading option) and with Pvcad

period	PVsyst near shading				PVsyst far shading				Pvcad			
	North	East	South	West	North	East	South	West	North	East	South	West
January	0.99	0.88	0.95	1.00	1.00	0.86	0.95	1.00	0.94	0.80	0.98	1.00
February	0.99	0.92	0.96	1.00	1.00	0.92	0.97	1.00	0.93	0.95	0.97	1.00
March	0.99	0.95	0.94	1.00	1.00	0.96	0.97	1.00	0.95	0.95	0.97	1.00
April	0.98	0.96	0.93	1.00	1.00	0.96	0.97	1.00	0.94	0.96	0.96	1.00
May	0.98	0.95	0.92	1.00	1.00	0.96	0.96	1.00	0.94	0.95	0.95	1.00
June	0.98	0.95	0.90	1.00	1.00	0.96	0.95	1.00	0.95	0.95	0.94	1.00
July	0.99	0.94	0.91	1.00	1.00	0.95	0.95	1.00	0.96	0.95	0.95	1.00
August	0.98	0.95	0.93	1.00	1.00	0.96	0.96	1.00	0.94	0.95	0.96	1.00
September	0.99	0.95	0.94	1.00	1.00	0.95	0.96	1.00	0.95	0.95	0.97	1.00
October	0.99	0.92	0.95	1.00	1.00	0.94	0.97	1.00	0.95	0.95	0.97	1.00
November	0.99	0.87	0.93	1.00	1.00	0.86	0.94	1.00	0.95	0.88	0.95	1.00
December	0.99	0.83	0.93	1.00	1.00	0.82	0.93	1.00	0.94	0.71	0.99	1.00
Annual	0.99	0.94	0.93	1.00	1.00	0.95	0.96	1.00	0.95	0.94	0.96	1.00
PVsyst: $b_0 = 0$; albedo 20%; albedo fraction 100%												

Appendix 5: Irradiation (reference cells), DC-energy and AC-energy per month and of one complete year

Period	MF	Hi-e kWh/m2	Hi-n kWh/m2	Hi-s kWh/m2	Hi-w kWh/m2	Edc-e kWh	Edc-n kWh	Edc-s kWh	Edc-w kWh	Eac-e kWh	Eac-n kWh	Eac-s kWh	Eac-w kWh
Jun/1999	90		46.3	70.3	94.5		15.7	28.0	38.4		12.2	23.8	33.3
Jul/1999	100		50.6	86.8	100.1		16.9	34.8	40.5		12.9	29.9	34.9
Aug/1999	100	64.6	37.2	89.5	86.0	25.1	12.8	36.3	34.6	20.9	9.3	31.4	29.8
Sep/1999	100	50.2	25.5	80.8	56.4	19.3	8.4	32.9	22.2	15.8	5.6	28.7	18.6
Oct/1999	89	28.9	15.4	77.8	37.3	10.6	4.7	31.8	14.2	8.1	2.5	27.7	11.5
Nov/1999	89	12.1	7.9	44.2	18.0	4.0	2.3	18.0	6.7	2.6	0.9	15.6	5.1
Dec/1999	88	7.5	6.1	28.3	10.6	2.2	1.7	11.2	3.6	1.1	0.6	9.4	2.4
Jan/2000	88	9.8	6.8	34.5	14.5	3.1	1.9	13.7	5.2	1.8	0.6	11.7	3.7
Feb/2000	100	22.0	12.6	63.0	27.9	7.9	3.8	25.7	10.4	5.9	2.0	22.4	8.3
Mar/2000	100	31.4	20.2	65.7	40.3	11.4	6.5	26.3	15.2	8.7	4.0	22.6	12.3
Apr/2000	96	55.9	28.4	83.4	58.7	21.6	9.4	33.7	22.9	17.9	6.4	29.2	19.0
May/2000	97	75.9	42.3	94.0	92.9	29.8	14.8	37.9	37.3	25.2	11.0	32.8	32.1
Jun/2000	100	80.8	50.0	85.6	101.5	31.9	18.1	34.2	40.9	26.9	14.1	29.3	35.3
Jul/2000	87	56.2	41.1	67.1	72.2	21.3	14.5	26.2	28.3	17.2	10.7	21.8	23.7
Aug/2000	100	76.4	38.2	107.5	93.9	30.2	13.2	44.1	38.0	25.7	9.6	38.7	32.8
Sep/2000	99	37.4	23.0	71.7	48.8	13.9	7.5	29.0	19.0	11.0	4.9	25.0	15.7
Oct/2000	100	17.8	13.0	41.6	26.2	6.0	4.0	16.4	9.7	4.0	2.0	13.7	7.5
Nov/2000	100	8.5	6.8	21.4	11.9	2.6	1.9	8.2	4.1	1.2	0.6	6.5	2.7
Dec/2000	100	8.4	6.2	31.1	12.0	2.5	1.7	12.3	4.1	1.2	0.5	10.3	2.7
Jan/2001	100	10.7	7.4	37.6	14.6	3.4	2.1	14.9	5.1	1.9	0.7	12.7	3.5
Feb/2001	79	16.7	11.0	46.3	24.4	5.8	3.3	18.7	9.1	4.0	1.7	16.1	7.2
Mar/2001	99	27.1	17.8	47.9	31.6	9.6	5.6	18.7	11.6	7.1	3.3	15.6	9.0
Apr/2001	100	59.2	30.9	82.0	66.6	22.9	10.4	33.0	26.1	19.1	7.3	28.5	22.1
May/2001	100	95.7	44.7	103.9	109.2	38.3	15.6	42.1	44.3	32.8	11.7	36.7	38.4
Feb/2000 - Feb/2001	97	481.4	289.3	769.6	600.8	182.7	97.5	308.9	235.0	146.9	66.7	265.0	195.7

Appendix 6: Efficiency data obtained from the data of appendix 5.

Period	eta_dc-e %	eta_dc-n %	eta_dc-s %	eta_dc-w %	eta_inv-e %	eta_inv-n %	eta_inv-s %	eta_inv-w %
Jun/1999		3.06	3.59	3.66		77.8	85.1	86.7
Jul/1999		3.01	3.62	3.65		76.3	85.7	86.2
Aug/1999	3.51	3.10	3.65	3.63	83.3	73.0	86.6	86.0
Sep/1999	3.46	2.98	3.67	3.54	82.2	67.0	87.1	83.9
Oct/1999	3.30	2.76	3.69	3.44	76.6	53.9	87.2	80.7
Nov/1999	2.99	2.60	3.67	3.33	63.9	40.4	86.5	76.1
Dec/1999	2.70	2.53	3.56	3.05	47.5	33.0	84.5	65.7
Jan/2000	2.86	2.52	3.59	3.22	56.4	32.4	85.0	71.8
Feb/2000	3.23	2.74	3.68	3.38	74.8	52.9	87.3	79.3
Mar/2000	3.27	2.88	3.61	3.41	76.5	62.3	85.7	80.8
Apr/2000	3.49	3.00	3.64	3.51	82.9	68.0	86.6	83.2
May/2000	3.54	3.16	3.64	3.62	84.4	74.6	86.6	86.0
Jun/2000	3.56	3.27	3.60	3.64	84.4	77.7	85.6	86.3
Jul/2000	3.42	3.17	3.52	3.53	80.7	74.2	83.3	83.7
Aug/2000	3.57	3.11	3.70	3.65	84.9	73.1	87.7	86.4
Sep/2000	3.36	2.96	3.65	3.51	78.9	65.4	86.3	82.8
Oct/2000	3.06	2.74	3.56	3.34	66.6	51.4	83.6	77.1
Nov/2000	2.74	2.54	3.43	3.10	48.3	32.7	79.5	65.9
Dec/2000	2.72	2.49	3.55	3.08	48.0	27.1	84.4	66.3
Jan/2001	2.85	2.53	3.58	3.14	56.5	33.0	85.2	69.3
Feb/2001	3.11	2.72	3.64	3.38	69.9	51.2	86.0	78.9
Mar/2001	3.21	2.83	3.52	3.32	73.8	58.4	83.2	77.3
Apr/2001	3.49	3.03	3.63	3.54	83.3	70.2	86.5	84.4
May/2001	3.61	3.15	3.65	3.66	85.8	74.7	87.0	86.6
Feb/2000 - Feb/2001	3.42	3.04	3.62	3.53	80.4	68.4	85.8	83.3

Appendix 7: Global irradiation, performance ratio, annual yield and normalised annual yield

Period	Ho	PR-e	PR-n	PR-s	PR-w
	kWh/m2	-	-	-	-
Jun/1999	160.13		0.52	0.67	0.70
Jul/1999	172.42		0.51	0.68	0.69
Aug/1999	139.48	0.64	0.50	0.70	0.69
Sep/1999	94.97	0.63	0.44	0.70	0.65
Oct/1999	56.73	0.56	0.33	0.71	0.61
Nov/1999	25.57	0.42	0.23	0.70	0.56
Dec/1999	16.16	0.28	0.18	0.66	0.44
Jan/2000	20.40	0.35	0.18	0.67	0.51
Feb/2000	43.43	0.53	0.32	0.71	0.59
Mar/2000	71.33	0.55	0.39	0.68	0.61
Apr/2000	108.80	0.64	0.45	0.69	0.64
May/2000	170.37	0.66	0.52	0.69	0.69
Jun/2000	181.37	0.66	0.56	0.68	0.69
Jul/2000	131.97	0.61	0.52	0.64	0.65
Aug/2000	162.35	0.67	0.50	0.71	0.69
Sep/2000	81.66	0.58	0.43	0.69	0.64
Oct/2000	41.43	0.45	0.31	0.66	0.57
Nov/2000	19.35	0.29	0.18	0.60	0.45
Dec/2000	17.63	0.29	0.15	0.66	0.45
Jan/2001	23.48	0.35	0.18	0.67	0.48
Feb/2001	35.86	0.48	0.31	0.69	0.59
Mar/2001	65.07	0.52	0.36	0.64	0.56
Apr/2001	121.44	0.64	0.47	0.69	0.66
May/2001	196.14	0.68	0.52	0.70	0.70
Between feb/2000 and feb/2001	1053.2	0.61	0.46	0.68	0.65
	Yield	291	132	526	388
	Norm. yield	277	126	499	369

Yield: Annual yield in kWh/kWp, based on 42 modules with a nominal power of 12 Wp
 Normalised yield: yield normalised to an annual global irradiation of 1000 kWh/m².

Appendix 8:

Calculated spectra (using SPECTRAL2, clear sky assumption) and measured spectra (normalised to the calculated spectra); Do = diffuse component of the global radiation.

